Supplementary material

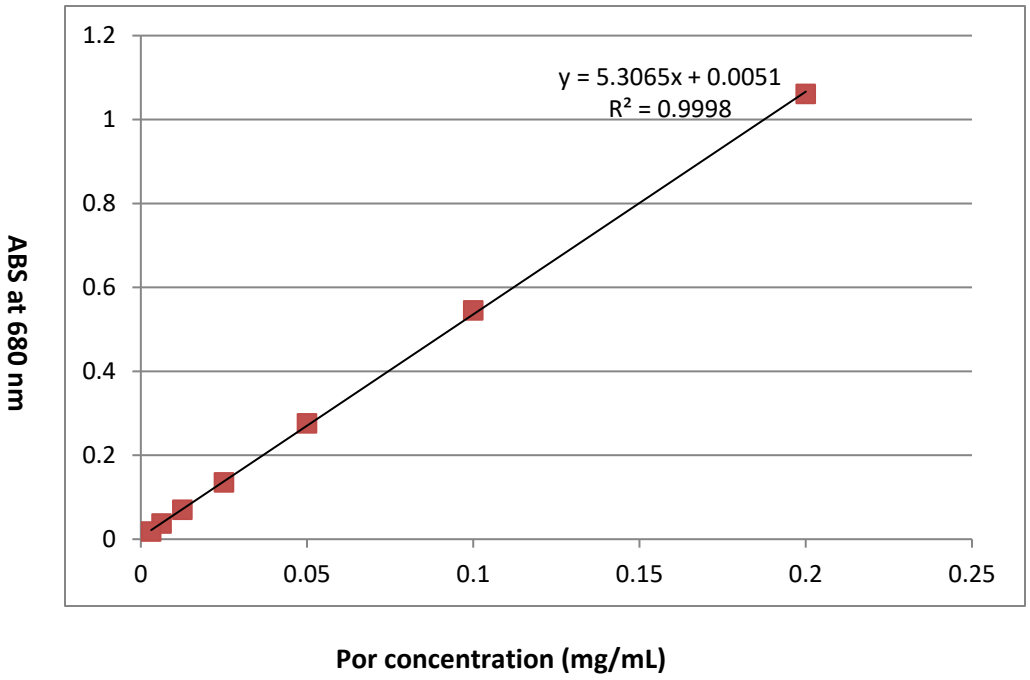

Figure S1. The calibration curve between the absorbance at 680 nm and concentrations of porphyrin standard measured by ultraviolet-visible spectroscopy.

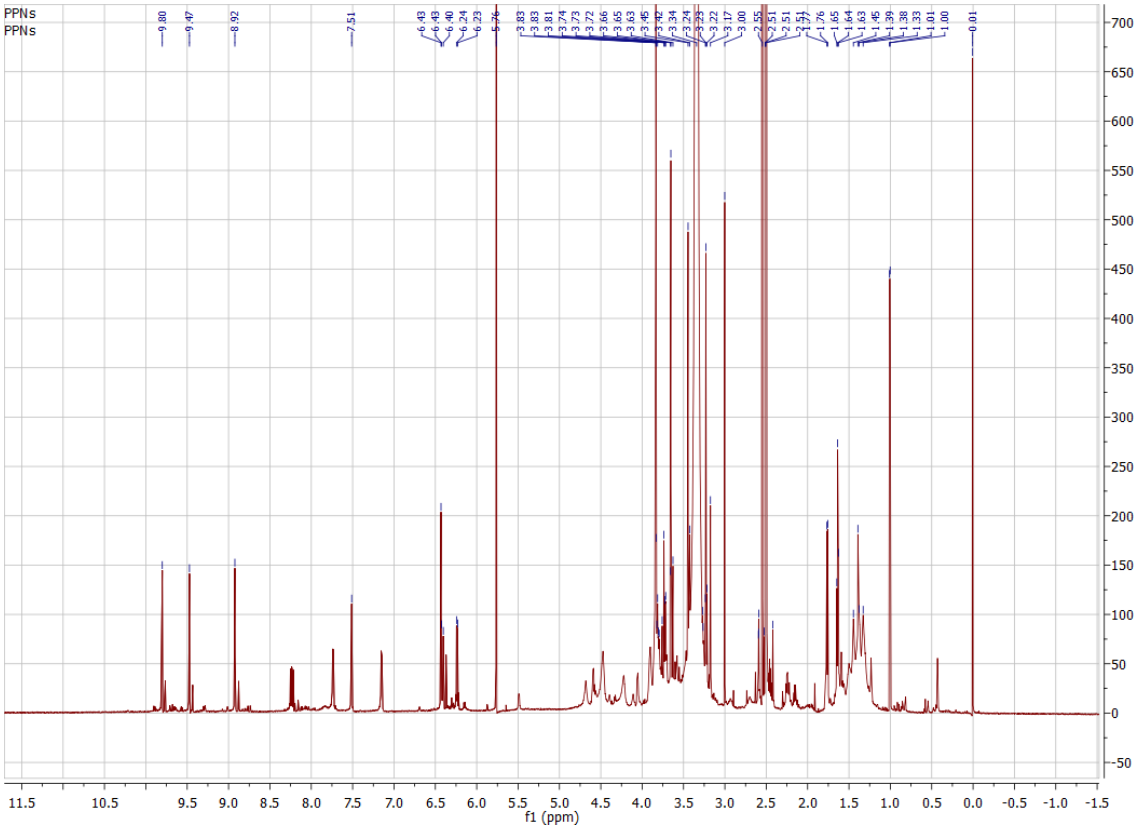

Figure S2. ^{1}H NMR spectra of PVA-porphyrin conjugate in DMSO-d6.

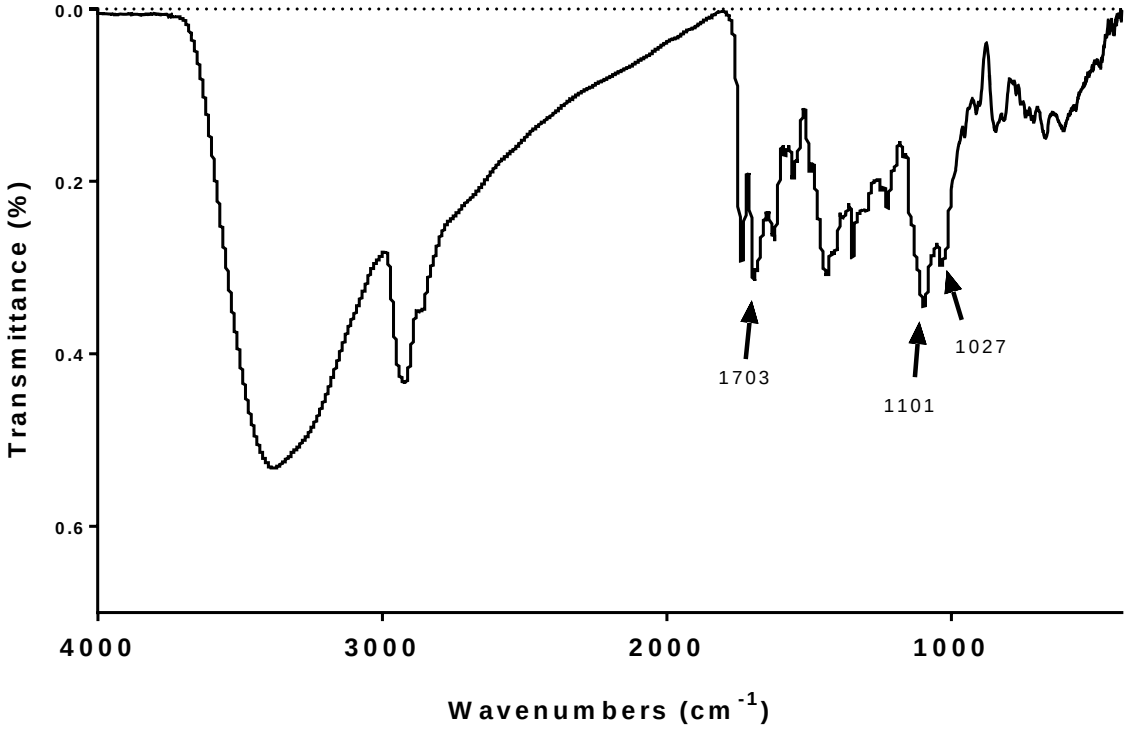

Figure S3. Fourier transform infrared spectroscopy (FTIR) spectrum of PVA-porphyrin conjugates.

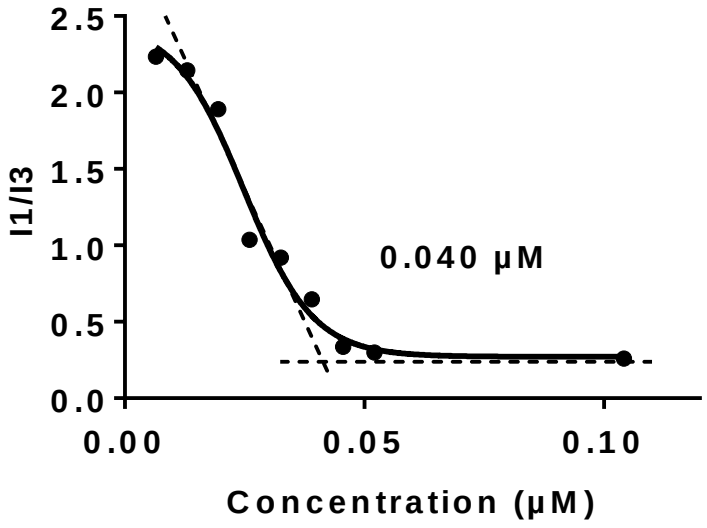

Figure S4. Critical micelle concentration of PVA-porphyrin conjugates measured by using pyrene as a probe.

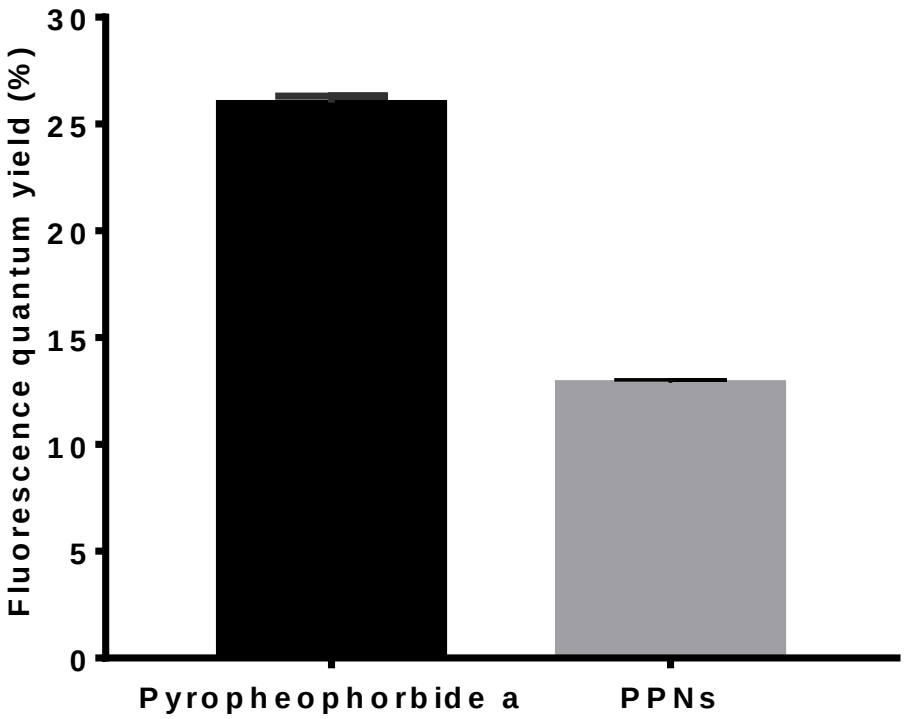

Figure S5. Fluorescence quantum yield of PPNs (ex 668 nm, em 720 nm).

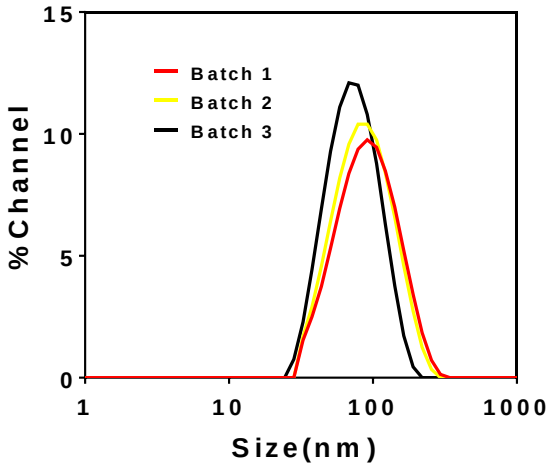

Figure S6. Batch-to-batch reproducibility of PPNs by measuring the variations in particle size.

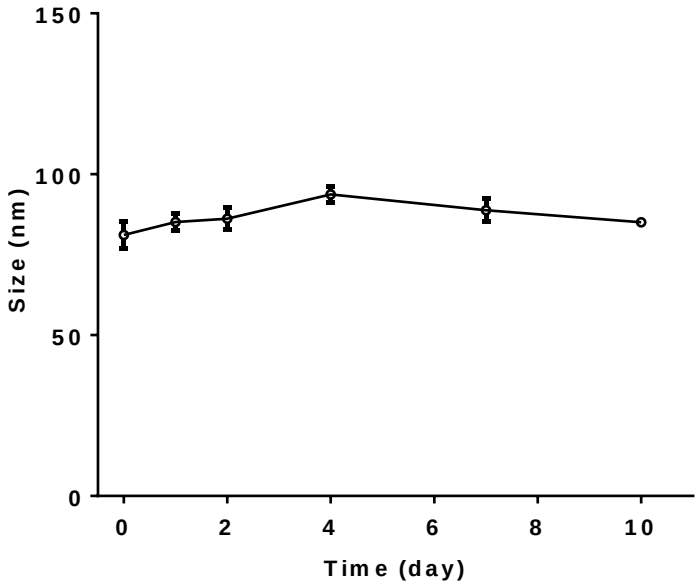

Figure S7. Stability studies of PPNs-DOX in cell culture medium with 10 % FBS by monitoring the changes in particle size.

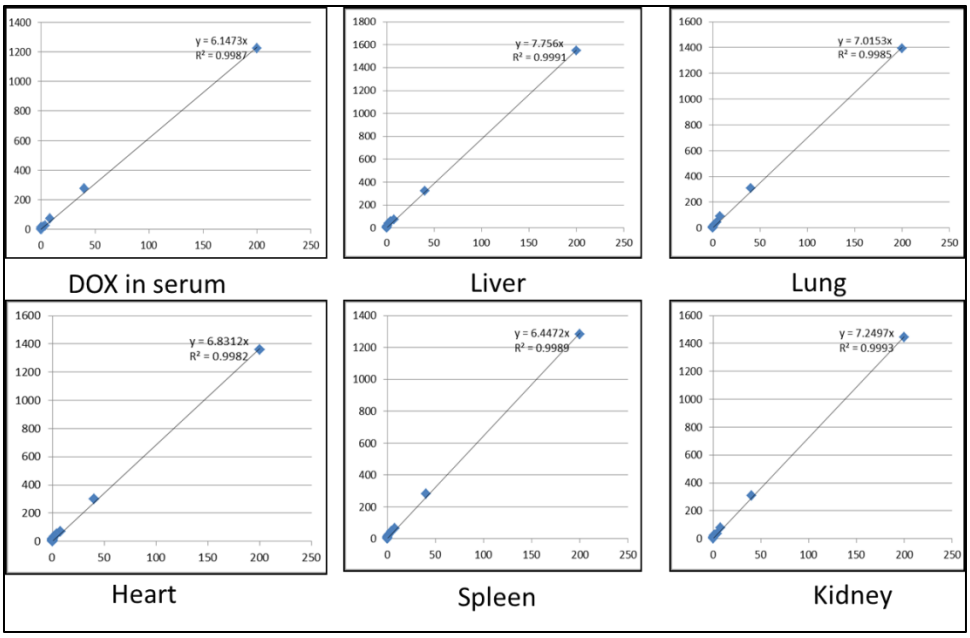

Figure S8. Calibration curve of DOX in serum and major organs of rats. Standard curves for DOX were generated to calculate their concentrations. To obtain the standard curve, free DOX with different concentrations were added to the plasma and organ homogenate followed by extraction and quantification.

	Free DOX	PPNs-DOX
$AUC_{0\text{-}24h}$(μg*min/ml)	5614±511	29241±424
Cmax calc	16.59±1.11	60.19±7.66
$T_{1/2\alpha}$(min)	1.43±0.03	76.26±41.62
Cl (ml/min/kg)	0.9±0.08	0.17±0.003

Figure S9. Pharmacokinetic study of PPNs-DOX in rats. The jugular vein of a male Sprague-Dawley rat was cannulated and a catheter was implanted for IV injection and blood collection. The catheter patency was maintained by flushing the catheter with sterile saline once a week. Free DOX and PPNs-DOX were injected through the catheter at a dose of 5mg/kg body weight, as well as equivalent dose of blank PPNs, respectively (n=2 for each group). Whole blood samples (approximately 200μl) were collected via jugular vein catheter before dosing and at 1, 3, 5, 15, 30, 60, 120, 240, 480 and 1440 minutes post-dosing. At each time point, about 50μl blood was drawn with a new syringe then discarded. Another new syringe took the 200μl of sample blood. Then 50μl of sterile saline was used to flush the catheter followed by 50μl of heparin in saline. The samples were immediately centrifuged and the plasma was separated and stored at -20℃ until analysis. 20μL of the plasma were added to 180μl extraction buffer (10% Triton X-100, deionized water and acidified isopropanol (0.75 N HCl) with volumetric ratio of 1:2:15), DOX was extracted overnight at -20℃. The fluorescence of DOX was determined at excitation/emission of 480/580 nm and 410/670 nm, respectively. The main pharmacokinetic parameters were obtained using non-compartmental analysis. The area under the plasma concentration-time curve (AUC) was calculated using the trapezoidal rule up to the last measureable drug concentration. Maximum concentration (C_{max}) and time to reach maximum concentration (T_{max}) were obtained directly from AUC. The half-life of the terminal phase ($t_{1/2}$) was calculated by $\ln(2)/k_e$. The total body clearance (Cl) was calculated by injected dose dividing AUC. Doses were normalized based on rat body weight.

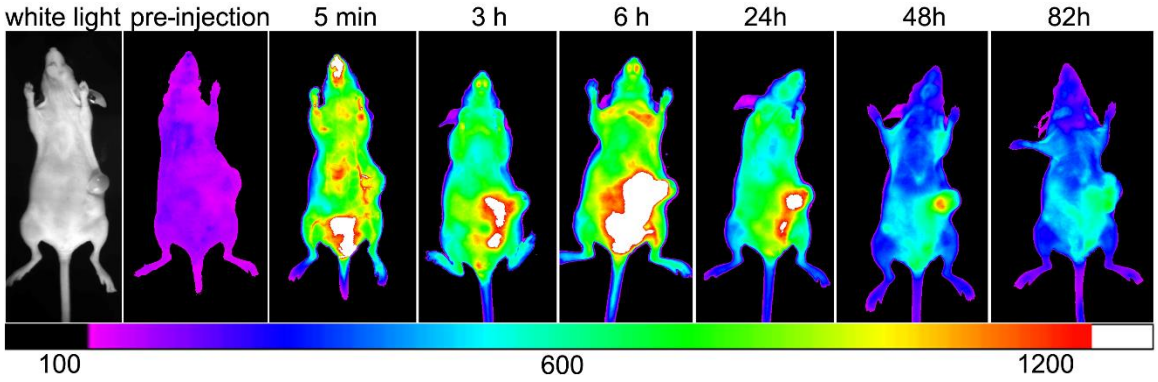

Figure S10. *In vivo* optical imaging of PPNs in SKOV-3 xenografts-bearing nude mice. For each mouse, 200 µl PBS solution of PPNs was injected via tail vein (n=5). At different time points (5 min, 3, 6, 24, 48 and 82 hrs) post-injection, mice were anesthetized by intraperitoneal injection of pentobarbital (60mg/kg), and scanned using Kodak multimodal imaging system IS2000MM with the excitation at 625 nm and the emission at 700 nm.

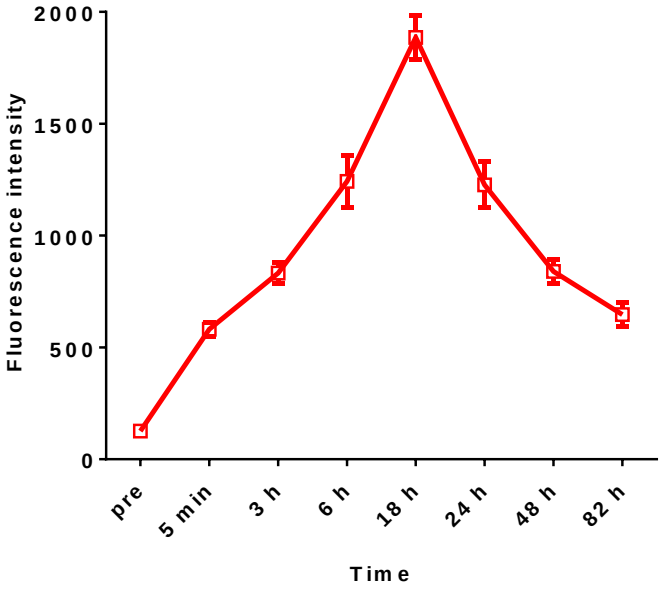

Figure S11. Semi-quantitative NIR fluorescence intensity of the *in vivo* SKOV-3 Tumor.

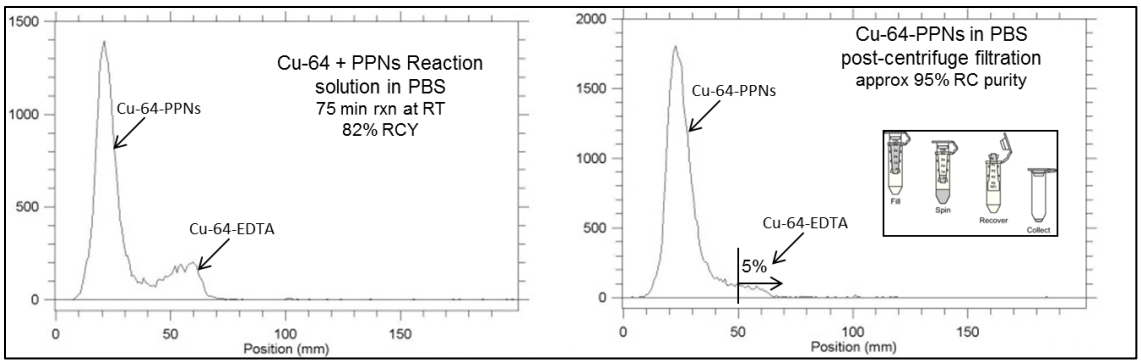

Figure S12. Evaluation of radiochemical purity and yield of ^{64}Cu-chelated PPNs by ITLC.

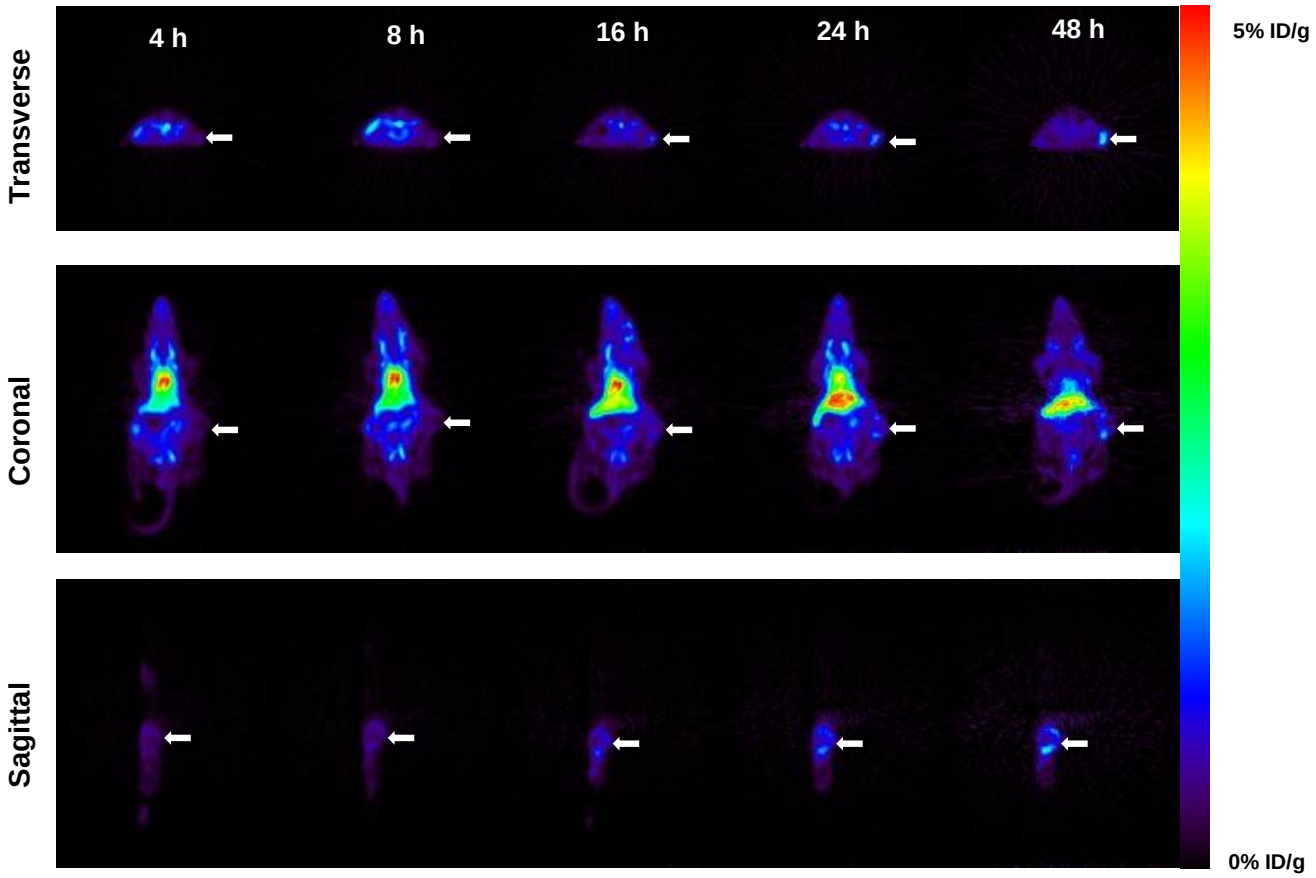

Figure S13. Represensitive PET images (Transverse, Coronal and Sagittal) of nude mice bearing SKOV3 ovarian cancer xenografts at 4, 8, 16, 24 and 48 h post injection of ^{64}Cu-labelled PPNs

(100 μl, ^{64}Cu dose: 0.5 mCi). The white arrow points to the tumor site. The tumor was found to be necrotic, which may explain why radio-uptake was low at the center of the tumor.

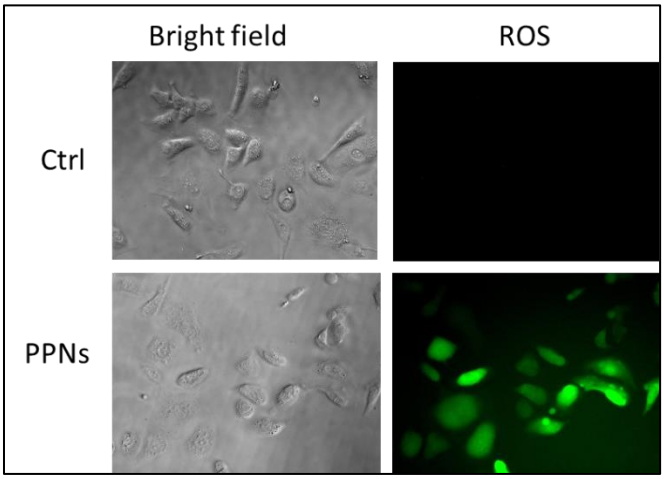

Figure S14. Evaluation of ROS production after PPNs-mediated PDT by fluorescence microscope. SKOV-3 cells were seeded in 6 well plates, and incubated with 8 ug/ml PPNs for 2h. Then remove the medium and wash thrice with PBS, add 1:500 ROS indicator and incubate for 20min. Then the cells were exposed to 30mW/cm^2 light for 2 min. Observe the cells under fluorescence microscope immediately.

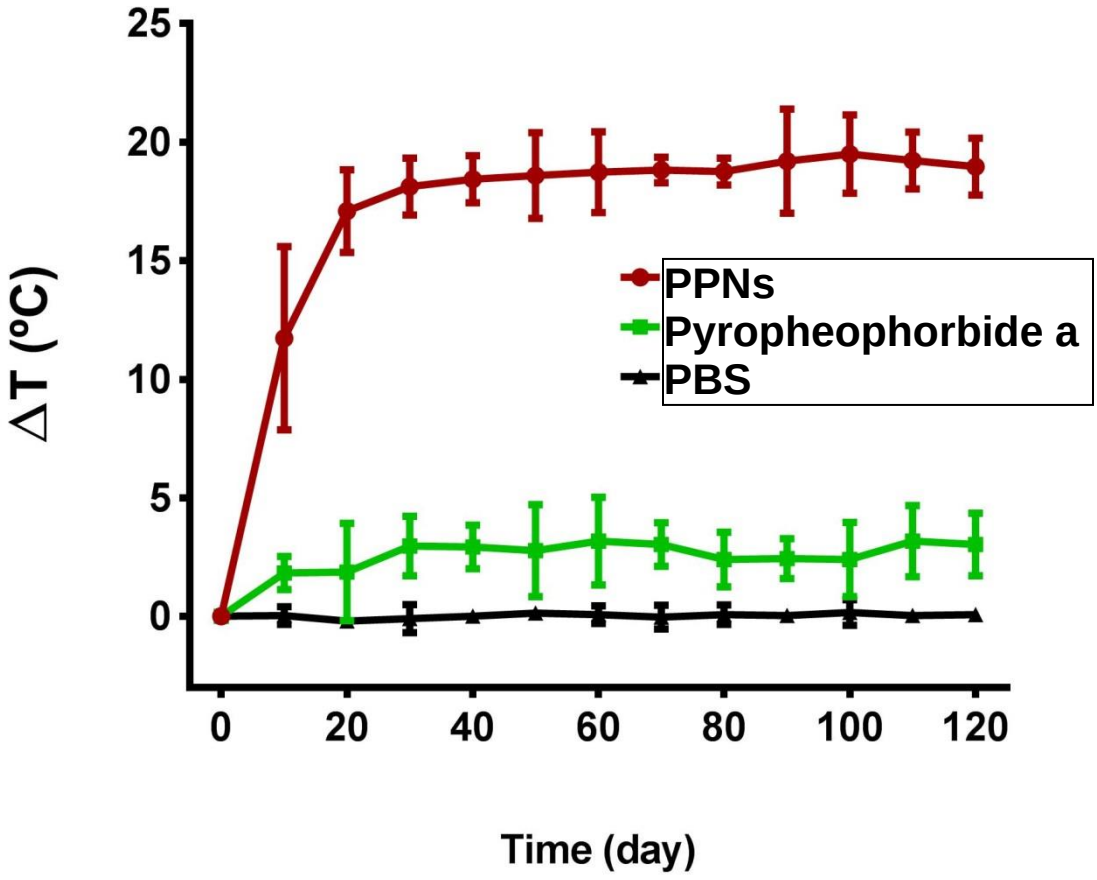

Figure S15. Photothermal conversion efficiency of PPNs, small-molecule pyropheophorbide a under the irradiation by 690 nm laser (0.5 W/cm^2) in 120 s.

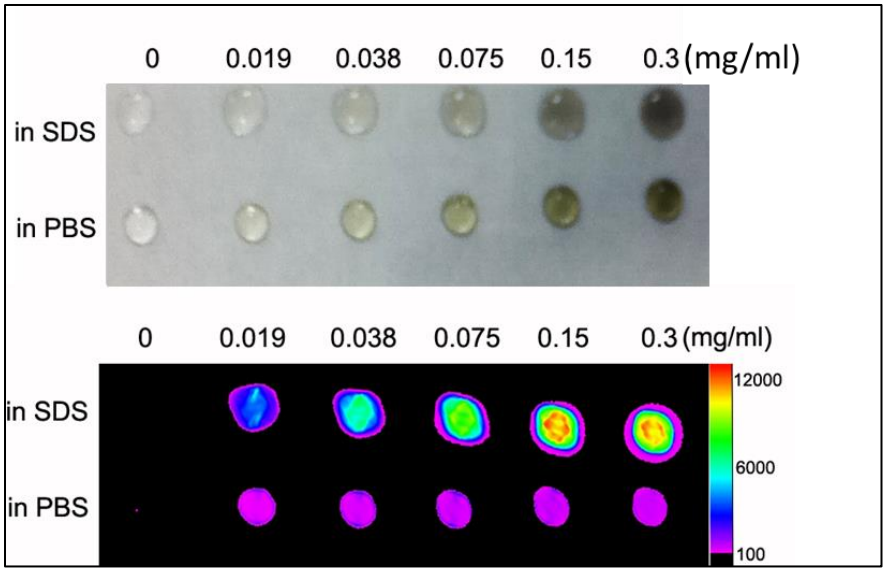

Figure S16. The bright field image of the drops of PPNs solution with or without SDS. NIFR fluorescence imaging of PPNs in the presence and absence of SDS, using an excitation filter at 625nm and an emission filter at 700 nm.

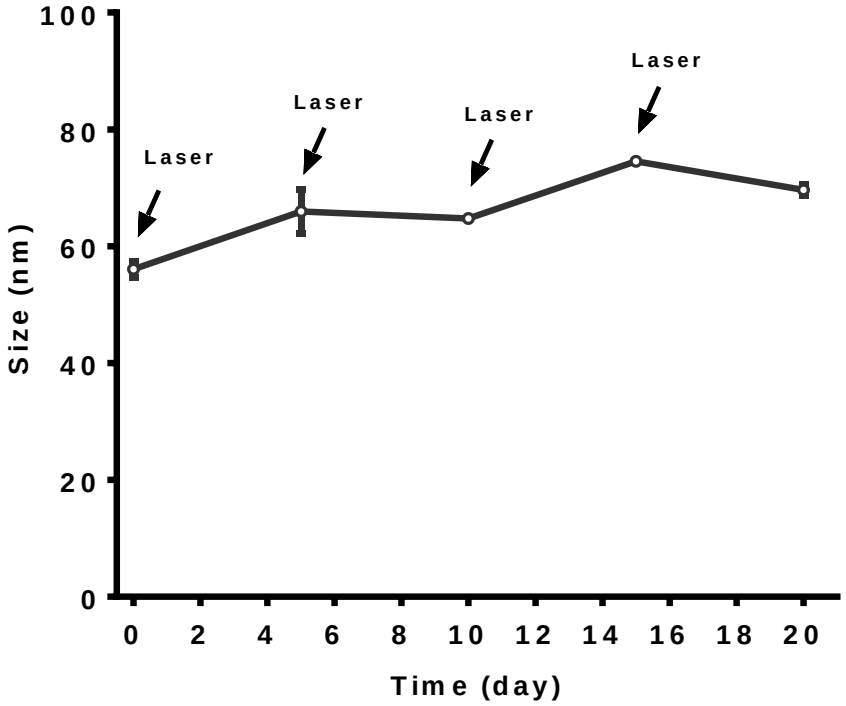

Figure S17. The photostability of PPNs-DOX with multiple irradiations. PPNs-DOX (1 mg/ml) was irradiated by 690 nm laser (0.5 W/cm^2) on day 0, 5, 10 and 15 for 2 min.